Biosensors and Bioelectronics 137 (2019) 271–278

Contents lists available at ScienceDirect

Biosensors and Bioelectronics

journal homepage: www.elsevier.com/locate/bios

Red-emitting FIT-PNAs: "On site" detection of RNA biomarkers in fresh human cancer tissues

Dina Hashoul[a,1], Rachel Shapira[b,1], Maria Falchenko[a,1], Odelia Tepper[a], Vera Paviov[b], Aviram Nissan[b,**], Eylon Yavin[a,*]

[a] School of Pharmacy, Faculty of Medicine, The Hebrew University of Jerusalem, Hadassah Ein-Kerem, Jerusalem, 91120, Israel
[b] Department of General and Oncological Surgery, The Chaim Sheba Medical Center, Tel Hashomer, Israel

ARTICLE INFO

Keywords:
Peptide nucleic acid
Long non-coding RNA
Hyperthermic intraperitoneal chemotherapy
CCAT1
KRT20

ABSTRACT

To date, there are limited approaches for the direct and rapid visualization (on site) of tumor tissues for pathological assessment and for aiding cytoreductive surgery. Herein, we have designed FIT-PNAs (forced-intercalation-peptide nucleic acids) to detect two RNA cancer biomarkers. Firstly, a lncRNA (long noncoding RNA) termed CCAT1, has been shown as an oncogenic lncRNA over-expressed in a variety of cancers. The latter, an mRNA termed KRT20, has been shown to be over-expressed in metastases originating from colorectal cancer (CRC). To these FIT-PNAs, we have introduced the bis-quinoline (BisQ) cyanine dye that emits light in the red region (605–610 nm) of the visible spectrum. Most strikingly, spraying fresh human tissue taken from patients during cytoreductive surgery for peritoneal metastasis of colon cancer with an aqueous solution of CCAT1 FIT-PNA results in bright fluorescence in a matter of minutes. In fresh healthy tissue (from bariatric surgeries), no appreciable fluorescence is detected. In addition, a non-targeted FIT-PNA shows no fluorescent signal after spraying this FIT-PNA on fresh tumor tissue emphasizing the specificity of these molecular sensors. This study is the first to show on-site direct and immediate visualization of an RNA cancer biomarker on fresh human cancer tissues by topical application (spraying) of a molecular sensor.

1. Introduction

Long non-coding RNAs (lncRNAs) are non-protein-coding transcripts of > 200 nucleotides. A variety of lncRNAs have been found to be differentially expressed in cancer (Huarte, 2015); with those acting as either oncogenic e.g. HOTAIR, MALAT1 (Huarte, 2015; Ji et al., 2003) or tumor suppressor genes e.g. GAS5 (Ma et al., 2016). It had become apparent in recent years that such lncRNAs have defined molecular mechanisms that influence the progression of the disease and thus may be excellent biomarkers for cancer diagnosis and prognosis. One of such lncRNA is CCAT1 (colon-associated transcript 1) (Guo and Hua, 2017; Nissan et al., 2012; Xin et al., 2016). CCAT1 is a 2682 nucleotides lncRNA that maps to chromosome 8q24.21. It is associated with a variety of cancers, including colon (Alaiyan et al., 2013), lung (Luo et al., 2014), gastric (Zhang et al., 2014), breast (Zhang et al., 2015), gallbladder (Ma et al., 2015), ovarian (Liu et al., 2013), and hepatocellular (Deng et al., 2015) cancers. Several studies have shown the prognostic value of CCAT1 for several indications (Luo et al., 2014; Nissan et al., 2012; Zhang et al., 2014).

KRT20 belongs to a family of proteins that form the intermediate filament cytoskeleton of epithelial cells. Its expression has been found in tumor cells located in peripheral blood (Wyld et al., 1998), bone marrow (Soeth et al., 1996), or lymph nodes (Futamura et al., 1998) originating from metastasis of patients with colon cancer.

The Seitz laboratory introduced the FIT-PNA concept in which one of the nucleobases (usually purines) is replaced with a "surrogate base" such as Thiazole Orange (TO) (Bethge et al., 2008; Koehler et al., 2005; Kummer et al., 2011). When TO is placed in the PNA strand, it is quenched due to intramolecular twisting of the dye in the excited state but gains fluorescence only after RNA/DNA hybridization. This is due to the change in the environment (viscosity) surrounding the probe (Silva et al., 2007). TO has also been used as a surrogate base in DNA as well as in DNA-LNA oligomers (Hoevelmann et al. 2014, 2016), where the surrogate base is flanked by LNAs leading to a dramatic increase in signal to background. In this regard, the Seitz group (Hoevelmann et al., 2016) and ours (Kolevzon et al., 2016) have recently developed a red-

* Corresponding author.
** Corresponding author.
E-mail addresses: Aviram.Nissan@sheba.health.gov.il (A. Nissan), eylony@ekmd.huji.ac.il (E. Yavin).
[1] The authors contributed equally to this article.

https://doi.org/10.1016/j.bios.2019.04.056
Received 22 January 2019; Received in revised form 15 April 2019; Accepted 29 April 2019
Available online 08 May 2019
0956-5663/

emitting surrogate base in DNA-LNA (QB = Quinoline Blue) and in PNA (BisQ = Bis Quinoline) oligomers, respectively.

We have used this approach as means for detecting point mutations in cancer by designing FIT-PNAs that target the KRAS oncogene and showed that this mRNA transcript can be detected and discriminated at a single nucleotide resolution in living cells (Kolevzon et al., 2016). This concept was further investigated by Wickstrom and co-workers in lung cancer (Sonar et al., 2014). Apart from detecting SNPs, FIT-PNAs have the capacity of detecting RNA in living cells as demonstrated for cells infected with viral mRNA (Kummer et al. 2011, 2012), miRNA (Torres et al., 2012), and lncRNAs (Kam et al., 2014).

Herein, we have designed and synthesized FIT-PNAs that turn on their fluorescence upon sequence-specific RNA hybridization. These probes were designed to target two RNA cancer biomarkers: CCAT1 and KRT20. We show the detection of CCAT1 and, to a lesser extent, KRT20 by their complementary FIT-PNAs in living cells. Importantly, we have been able to unveil that spraying the specific CCAT1 FIT-PNA probe directly on fresh (un-fixed) cancerous human tissue from surgical procedures (cytoreductive surgery) results in a bright fluorescent signal in a short time interval (minutes). KRT20 FIT-PNA shows a weaker fluorescence and slower response. No fluorescent signal is observed after spraying these FIT-PNAs with healthy fresh tissue taken from bariatric surgeries or when spraying a non-specific FIT-PNA on cancerous fresh tissue.

This approach opens a simple and straight forward methodology to detect RNA biomarkers in fresh tissues simply based on the design of the FIT-PNA probe that complements the RNA biomarker of choice. The detection is observed within minutes after spraying a buffered solution of the FIT-PNA directly on the malignant fresh tissue.

2. Materials and methods

2.1. General

Manual solid-phase synthesis was performed by using 5 mL polyethylene syringe reactors (Phenomenex) that are equipped with a fritted disk. All column chromatography was performed using 60A, 0.04–0.063 mm Silica gel (Biolab, Israel) and manual glass columns. TLC was performed using Merck Silica Gel 60 F254 plates. HPLC purifications and analysis were performed on a Shimadzu LC-1090 system using a semi-preparative C18 reversed-phase column (Jupiter C18, 5μ, 300Å, 250 × 10mm, Phenomenex) at 50 °C. Eluents: A (0.1% TFA in water) and B (MeCN) were used in a linear gradient (11–40 %B in 30 min) with a flow rate of 4 mL/min. NMR spectra were recorded on a 300 MHz Bruker NMR using deuterated solvents as internal standards. MS measurements of compounds 1–5 and BisQ were measured on a ThermoQuest Finnigan LCQ-Duo ESI mass spectrometer. Mass analysis of BisQ-FIT-PNA was acquired on a MALDI-TOF MS. DNA and RNA oligos were purchased from Sigma-Aldrich, Israel. Dry DMF was purchased from Acros and Fmoc/Bhoc protected PNA monomers from PolyOrg Inc. (USA). The Fmoc-protected amino acids and reagents for solid phase synthesis were purchased from Merck (Germany).

2.2. Synthesis of PNA monomer with BisQ

Fmoc-Aeg-(BisQ)-O-allyl was synthesized as previously described (Kolevzon et al., 2016; Sonar et al., 2014) with slight modifications. To a solution of the dried reaction mixture of BisQ-CH_2COOH in 7 mL dry DMF, PyBOP (825 mg, 1.2 eq), HOBt (250 mg, 1.2 eq) and N-methylmorpholine (0.18 mL, 1.2 eq) were added. The reaction mixture was stirred at 0 °C for 15 min under argon. To this solution, a separately prepared mixture of Fmoc-Aeg-O-allyl (720 mg, 1.2 eq) and NMM (0.18 mL, 1.2 eq.) in DMF (1 mL) was added and the reaction mixture was allowed to stir for 12 h at RT. When the reaction was complete (as indicated by TLC), the reaction mixture was diluted with water prior to extraction with EtOAc (3 × 20 mL). The combined organic layers were washed with 10% $NaHCO_3$ followed by washing with 10% citric acid. The combined organic layers were washed again with aqueous 10% $NaHCO_3$ followed by water and brine. The organic layer was dried over anhydrous Na_2SO_4 and concentrated under vacuum. The crude product was column purified (silica gel) using 3–10% chloroform in DCM. (Yield = 70%)

^{1}H NMR (DMSO-d_6): 9.30 (br s, 2H)): 8.73 (d, 1H, ArH), 8.63 (d, 1H, ArH), 8.32 (m, 1H, ArH), 7.88 (d, 2H), 7.68 (d, 2H), 7.52 (t, 1H), 7.41 (t, 2H), 7.32 (t, 2H), 5.92 (dt, 1H), 5.24–5.39 (dd, 2H), 4.69 (d, 2H), 4.33 (d, 2H), 4.21 (t, 1H), 4.05 (br s, 2H), 3.31 (q, 2H), 3.01 (br s, 2H), 3.60 (t, 1H, N–CH2), 3.39 (m, 2H, N–CH2), 3.14 (m, 1H, N–CH2), 4.02 (s, 1.4H, Gly-CH2), 3.60 (t, 1H, N–CH2), 3.39 (m, 2H, N–CH2), 3.14 (m, 1H, N–CH2). MS: Mobs = 705.8, Mcalc = 705.31.

To a solution of Fmoc-Aeg (Dye)-O-allyl (370 mg) in DCM (10 mL) was added N-methylaniline (1 eq.). The solution was degassed by bubbling with argon for 5 min. After addition of [$Pd(PPh_3)_4$] (0.1 eq.), the mixture was stirred under exclusion of light for 14 h diethyl ether (30 mL) was added to precipitate the product which was collected by filtration and used without further purification. (Yield = 68%)

^{1}H NMR (DMSO-d_6): 8.73 (d, 1H, ArH), 8.63 (d, 1H, ArH), 8.32 (m, 1H, ArH), 7.97–7.87 (m, 5H, ArH), 7.71 (m, 5H, ArH), 7.56 (m, 3H, ArH), 7.41 (t, 2H, ArH), 7.31 (t, 2H, ArH), 7.26 (s, 1H, CH), 5.55 (s, 1H, CH2), 5.33 (s, 1H, CH2), 4.37 (m, 1H, Fmoc-CH2), 4.35 (s, 0.5H, Gly-CH2), 4.30 (d, 1H, Fmoc-CH2), 4.24 (t, 0.5H, Fmoc-CH), 4.20 (t, 0.5H, Fmoc-CH), 4.12 (s, 3H, N + -CH3), 4.02 (s, 1.4H, Gly-CH2), 3.60 (t, 1H, N–CH2), 3.39 (m, 2H, N–CH2), 3.14 (m, 1H, N–CH2). HRMS: Mobs = 665.275, Mcalc = 665.275.

2.3. Solid-phase synthesis of BisQ-FIT-PNA

The general procedures were published and are detailed elsewhere (Kolevzon et al., 2016).

2.4. Fluorescence of FIT-PNAs in a buffered solution

Fluorescence spectra were recorded by using a Jasco FT-6500 spectrometer.

Measurements were carried out in fluorescence quartz cuvettes (10 mm) at 0.5–1.5 μM concentration in a PBS buffered solution (100 mM NaCl, 10 mM NaH_2PO_4, pH 7). Quantum yields were determined relative to rhodamine B in PBS as described (Kovaliov et al., 2013). FIT-PNA (1 μM) was hybridized to its complementary RNA by heating a 1:1 mixture of PNA: RNA (1.5 μM) to 95 °C for 2 min followed by slow cooling to 25 °C. Samples were excited at 590 nm and emission spectra were recorded at 600–800 nm.

2.5. Cell lines and culture

Two cell lines were used: HT-29 (human colon adenocarcinoma grade II), and SK_Mel2 (human malignant melanoma).

Cell lines were purchased from the American Type Culture Collection (ATCC, Manassas, VA, USA). HT-29 expressing the lncRNA CCAT1 and KRT20 mRNA were cultured (37 °C, 5% CO_2), in DMEM medium and supplemented with 10% fetal calf serum, 2 mM L-glutamine, and 0.1 mg/mL Streptomycin (Beit Ha-Emek Biological Industries, Israel).

SK_Mel2 (used as controls) were cultured in RPMI medium supplemented with 10% fetal calf serum, 2 mM L-glutamine and 0.1 mg/ml streptomycin.

2.6. Cellular uptake analysis

Twenty-four hours prior to FIT-PNA addition, cells were plated separately on chamber slides (Ibidi GmbH, Munich, Germany) until reaching 70–80% confluence.

2.7. Hybridization and imaging in living cells

Before adding the FIT-PNA, the medium was replaced and the cells were incubated (37 °C, in a humidified atmosphere containing 5% CO_2) with 1 μM of FIT-PNA in complete medium. Cells were washed with PBS (× 3) prior to cell imaging and the intracellular fluorescence was measured after 2 h by confocal microscopy. (Olympus, FM 300, Japan, objective: UPIanApo 40X/1.0 oil, laser wavelength 633 nm).

2.8. Tissue RNA extraction

All tissues were thoroughly crushed on dry ice and disrupted with 1 mL per 50–100 mg tissue, denaturizing lysis buffer using a polytron® tissue homogenizer. RNA was extracted using TriReagent® protocol according to the manufacturer recommendations (Bio-Lab™). The RNA concentration was measured with NanoDrop® Spectrophotometer (ND-1000, NanoDrop Technologies™, Wilmington, DE (and stored at −80 °C until use).

2.9. Cell lines- RNA extraction

Cell lines were cultured (37 °C, 5% CO2) in DMEM or EMEM media. About 10 million cells were incubated in Trypsin EDTA solution B (Biological Industries, Israel). The media was removed after 3–5 min (at 37 °C) to disconnect the cells from the flasks' surface. Cells were washed with PBS and RNA was extracted using TriReagent® protocol as mentioned above.

2.10. CCAT1 and KRT20 qRT-PCR analysis

1 μg of total RNA extracted from different cell lines was used for reverse transcription with random primers in a 20 μl reaction of which 2 μl was used for polymerase chain reaction (PCR). All experiments were conducted in duplicates. qRT-PCR was performed for 40 cycles (denaturation: 95 °C × 15 s; annealing/extension: 60 °C × 1 min) with the primers and TaqMan® probe specific for human GAPD (GAPDH). The GAPDH endogenous control (VIC/MGB Probe, Primer Limited, 4326317E) was obtained from Applied Biosystems, Foster City, CA, USA.

For CCAT1 expression analysis, the primers and probe used were:

- Forward primer: 5′-TCACTGACAACATCGACTTTGAAG;
- Reverse primer: 5′-GGAGAAAACGCTTAGCCATACAG;
- Probe: 6Fam-CTGGCCAGCCCTGCCACTTACCA-Tamra.

For KRT20 expression analysis, the primers and probe used were:

- Forward primer 1 5′-TCC AGT CCC ATC TCA GCAT-3′
- Revers primer 5′-GCG TTC CAT GTT ACT CCG AAT-3′
- 6-Fam/CAG CCA GTT/Zen/AGC CAA CCT CCA GT/3IABkFQ/-3′

Relative quantification was done according to the manufacturer's instructions (Applied Biosystems, Foster City, CA, USA; User Manual 2). Each sample was normalized according to its GAPDH content and also against a calibrator set constructed of RNA obtained from normal colon tissue (AmbionVR Austin, TX, USA).

All experiments were performed using an ABI Prism 7500 system (Applied Biosystems, Foster City, CA, USA).

2.11. FIT-PNA hybridization in fresh human biopsies

Human peritoneal metastatic tissues were taken from Cytoreductive Surgery- Hyperthermic Intraperitoneal Chemotherapy (CRS-HIPEC). In addition, bariatric surgeries (normal tissues) were chosen for this study (surgeries were conducted at the Sheba Medical Center, Ramat-Gan, Israel). Tissues were cut into two pieces in order to be used for FIT-PNA hybridization and RNA isolation. The specimens for the hybridization were washed with Dulbecco's phosphate buffered Saline (1XPBS) twice, for 5 min. Afterward the samples were left in PBS for about 1.5 h until further analysis (spraying FIT-PNA and imaging). After the samples were cut and placed on cover slip slides, the samples were sprayed with the FIT-PNA solution (2.5 μM in PBS) and immediately imaged on a confocal microscope (Olympus, FM 300, Japan, objective: UPIanFI 10X/0.3, laser wavelength 633 nm).

2.12. Deep tissue imaging

Fresh tissues were sprayed with the FIT-PNA solution (2.5 μM in PBS) and immediately imaged on a multiphoton microscope (Nikon A1MP, objective: CFI75 Apo 25xW MP (NA 1.10 WD 2.0)), laser excitation = 540 nm, and emission = 601-657. For all cases, tissues were cut into two pieces. The segments used for RNA isolation, immediately following surgical resection, were snapped frozen in liquid nitrogen for further RNA extractions.

3. Results

3.1. FIT-PNA design and photophysical properties

The synthesis of a Fmoc-protected PNA monomer where the natural base is replaced with a surrogate base allows the selective introduction of the fluorophore at a desired location on the PNA sequence. The red-emitting BisQ surrogate base was introduced on a PNA backbone (Supplementary Scheme S1) consisting of Fmoc and allyl protecting groups (Sonar et al., 2014). Subsequently, FIT-PNAs targeting CCAT1 and KRT20 were synthesized on the solid phase as previously reported (Supplementary Table S1 and Figs. S1–S6) and their structures are shown in Scheme 1 (Kolevzon et al., 2016). The CCAT1 sequence was chosen based on our previous work (Kam et al., 2014). Two KRT20 FIT-PNA probes were designed and synthesized based on the UNAfold software (http://unafold.rna.albany.edu). We have used only one of these probes (Table S1), as we have seen no fluorescence in KRT20 expressing cells (HT-29) after incubation with the latter FIT-PNA probe (data not shown).

Fluorescence enhancement of FIT-PNAs were measured for fully complementary RNA sequences (Supplementary Fig. S7 and Fig. S8). For CCAT1 and KRT20 – a ca. 12 and 20 fold enhancement in fluorescence was shown for complementary RNA, respectively.

Table 1presents the physical properties of FIT-PNAs in single strand form and in duplex form with a fully complementary RNA. ε and ϕ values for both duplexes result in high brightness (εxϕ) that is only ca. 2.5 fold lower than that of Cy5.

3.2. FIT-PNAs fluoresce in living cells

The FIT-PNAs fluorescence in living cells were also explored. Fig. 1 presents typical confocal images of cancer cells that either over-express (HT-29, a colon cancer cell line) or have negligible (SK_Mel2, a melanoma cell line) CCAT1 RNA expression as determined by quantitative RT-PCR (Table S2). A short incubation period of 2 h with 1 μM CCAT1-

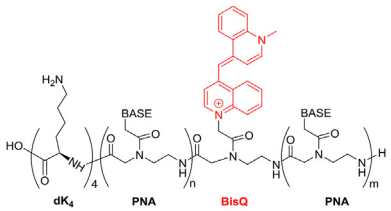

Scheme 1. Chemical structures of FIT-PNAs.

Table 1
Photophysical properties of FIT-PNAs.

Compound	λ_{max} abs (nm)	ε_{max} [$M^{-1}cm^{-1}$]	λ_{max} em (nm)	ϕ
CCAT1 FIT-PNA	593	81,667	n.a.	n.a.
CCAT1 FIT-PNA:RNA	592	95,833	610	0.27
KRT20 FIT-PNA	584	58,200	n.a	n.a
KRT20 FIT-PNA:RNA	586	103,000	608	0.315

FIT-PNA resulted in a clear fluorescence in cells expressing this RNA biomarker (HT-29, Fig. 1). In contrast, negligible fluorescence was found when these FIT-PNAs were incubated with SK_Mel2 cells (Fig. 1).

A weak signal was observed for KRT20-FIT-PNA (1 μM) (Supplementary Fig. S9) after a 2 h incubation with HT-29 cells that express this mRNA (Supplementary Table S2). Nonetheless, this FIT-PNA showed no apparent fluorescence in a control cell line (SK_Mel2) that has low expression of KRT20 mRNA (Supplementary Table S2). It is possible that this specific FIT-PNA sequence is not the ideal one for KRT20 mRNA detection and that others may be explored.

Interestingly, this fluorescent signal for CCAT1 FIT-PNA (in HT-29 cells, Fig. 1) was achieved by introducing a very short positively charged peptide (4 D-lysines) conjugated to the C-terminus of this FIT-PNA. We have already shown that this short peptide is sufficient for FIT-PNA delivery into living cells (Kolevzon et al., 2016).

To further validate the sequence-specificity of the FIT-PNAs, we have incubated a non-related FIT-PNA (Supplementary Table S1, Fig. S5, and Fig. S6) in the HT-29 cell line as a control. This FIT-PNA has no sequence homology to the human transcriptome and has the same peptide ($(D\text{-}Lys)_4$) on its C-terminus (Supplementary Table S1). The addition of this FIT-PNA at 1 μM for 2 h resulted in negligible fluorescence (Supplementary Fig. S9) which further supports the specificity of both FIT-PNAs to their designed RNA targets (CCAT1 and KRT20).

3.3. FIT-PNAs fluoresce in human fresh tumor tissues

Colorectal cancer (CRC) is a disease that typically progresses in years. If diagnosed early on, CRC patients have over 90% 5 years (and over) survival rate. CCAT1 is highly expressed in CRC (Nissan et al., 2012). Treatment of peritoneal metastasis originating from colon cancer by cytoreductive surgery (CRS) followed by hyperthermic intraperitoneal chemotherapy (HIPEC) consists of resection of all macroscopic tumor deposits and treating microscopic residual disease by washing the peritoneum with a warm (42 °C) solution of cytotoxic drugs, achieving high local concentrations of the drugs while keeping systemic drug levels low. This procedure has been shown to extend the survival rate of patients (Verwaal et al., 2003). However, early disease recurrence occurs in 30%–40% of treated patients and is mainly due to occult metastasis not identified by the surgeon.

Fluorescence-guided surgery (FGS) is a procedure used to maximize tumor excision by detecting in a real-time manner occult metastasis thereby improving survival rates of patients (Dsouza et al., 2016; Hague et al., 2017; Low et al., 2018; Wang et al., 2018; Zhang et al., 2017). In the context of CRS-HIPEC, in a recent clinical study (Harlaar et al., 2016), a mAb-targeted near IR dye (bevacizumab-IRDye800CW) was administered I.V. to 7 patients prior to surgery of peritoneal carcinomatosis. In two patients, the surgeon detected additional cancerous tissue by the aid of FGS. In general, the probe in FGS is injected systemically prior to surgery and is constantly fluorescent.

The study protocols presented herein were approved by the Institutional Independent Ethical Committee (IEC, Helsinki committee, #2200–15). Patients undergoing CRS-HIPEC for peritoneal metastasis were offered participation in this study in order to explore the possible use of FIT-PNAs for detecting the CCAT1 and KRT20 biomarkers in fresh human tissue. Fresh tissue samples obtained from the operating room were sliced into two. One slice was stored in PBS at RT and was used for fluorescence imaging. The other was frozen for qRT-PCR analysis. The fresh (un-frozen) cancerous tissues were sliced to about 1 mm (thickness) and placed directly on a glass slide. An aqueous solution of 2.5 μM FIT-PNA (for either CCAT1 or KRT20) was prepared in a spraying bottle. Fresh cancerous tissues were then sprayed twice (about 100 μLX2 per sample) with this FIT-PNA solution and confocal images were acquired at different time points (Fig. 2a and b and Fig. 2c and d for CCAT1 (two patients) and KRT-20 (two patients), respectively). These experiments were repeated for both FIT-PNAs and are shown in supporting information (Supplementary Fig. S10 and Fig. S11). In all cases, bright fluorescence was observed for all HIPEC fresh tissues examined, with CCAT1 FIT-PNA showing brighter images as also observed for the HT-29 cell line (Fig. 1).

Notably, fresh tumor tissues showed distinct and bright red fluorescence even at time zero for CCAT1-FIT-PNA (Fig. 2a and b) which is the time from spraying the sample until acquiring a confocal image (2–3 min).

To verify these results, the other (frozen) tissues taken from the same biopsy were analyzed by qRT-PCR for CCAT1 and KRT20 levels (Table 2 and Supplementary Table 3S). A positive RQ value was found for all tumor tissues (for both RNA biomarkers) providing a qualitative verification of these biopsies as of tumor origin.

In addition, and as a control, another tissue type was evaluated post-surgery, namely, fresh normal tissues from patients undergoing bariatric surgery. These fresh normal tissues were imaged after spraying a 2.5 μM solution of either CCAT1 or KRT20 FIT-PNAs (Fig. 3a and b and Fig. 3c and d for CCAT1 and KRT20, respectively, and repeated experiments in supporting information (Supplementary Fig. S12)). In all cases, no appreciable fluorescence was detected. As with the HIPEC

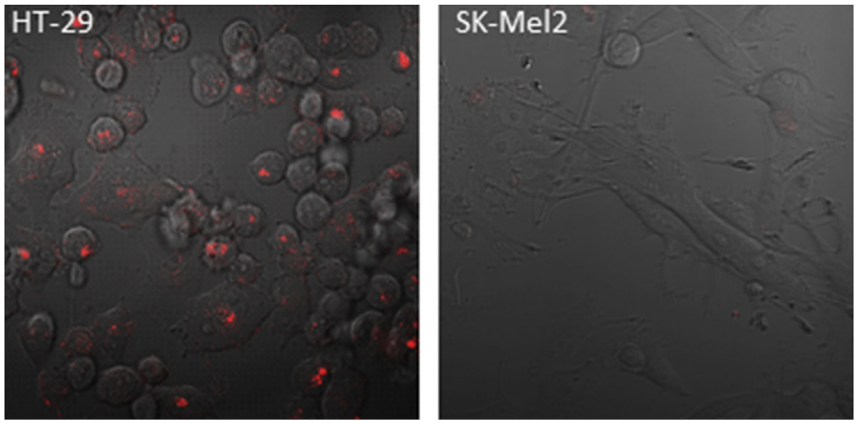

Fig. 1. BisQ-FIT-PNA detects CCAT1 lncRNA in living cells. Confocal microscopy images of cancer cell lines incubated with 1 μM CCAT1 FIT-PNA (red). Images were acquired after 2 h incubation at 37 °C.

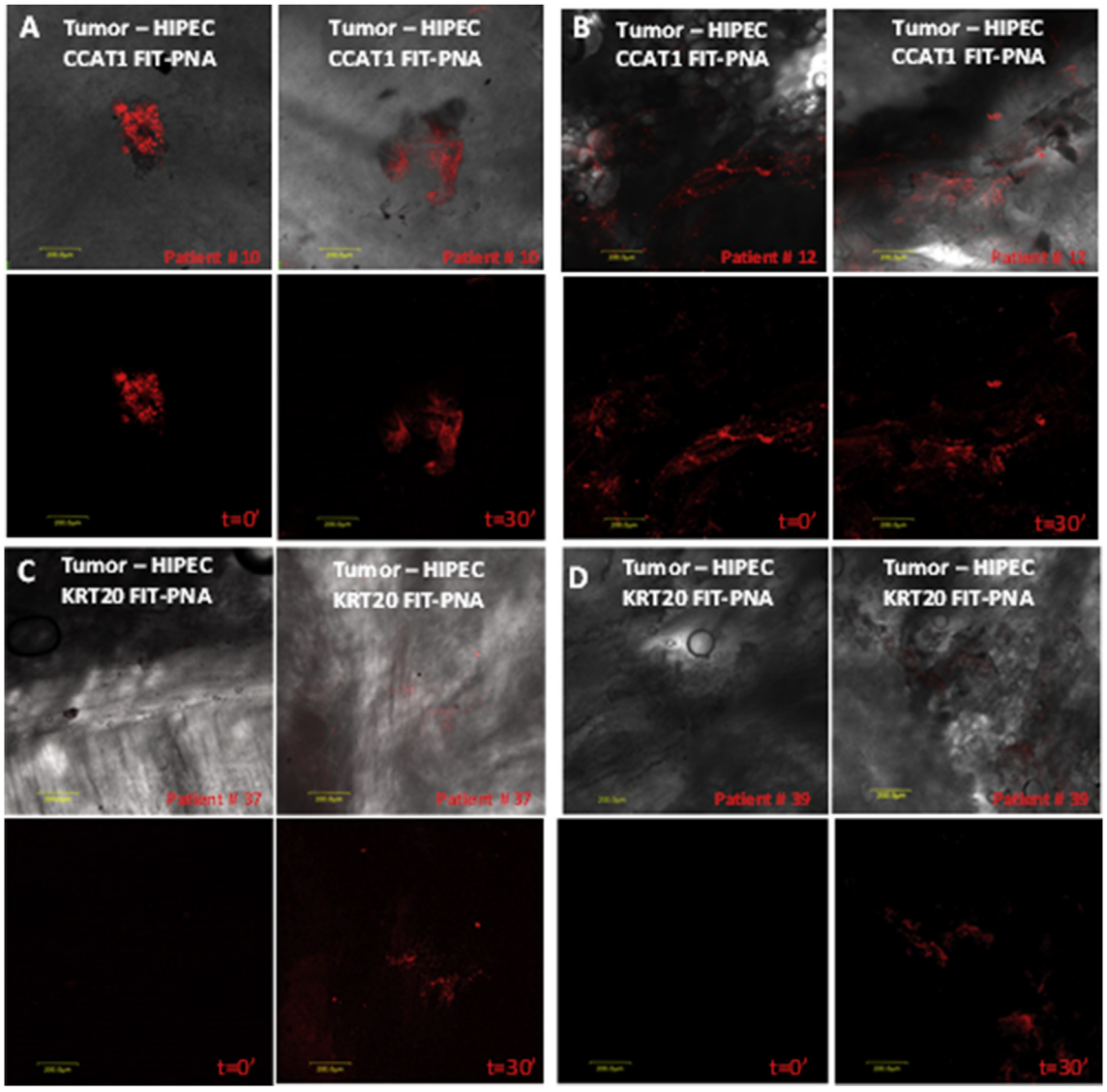

Fig. 2. FIT-PNAs fluoresce after direct spraying on fresh human tumor tissue. a) and b) Peritoneal metastatic tissue after CRS-HIPEC from 2 patients after spraying tissues with 2.5 μM CCAT-FIT-PNA, c) and d) Peritoneal metastatic tissue after CRS-HIPEC from 2 patients after spraying tissues with 2.5 μM KRT20-FIT-PNA. Scale bar – 200 μm.

Table 2
Relative quantification (RQ) of CCAT1 and KRT20 RNA levels in tissues as determined by qRT-PCR.

Patient #	Tissue type	RNA detected	RQ values
10	HIPEC (Tumor)	CCAT1	49.9
12	HIPEC (Tumor)	CCAT1	427.9
41	HIPEC (Tumor)	CCAT1	8.1
37	HIPEC (Tumor)	KRT20	7631
39	HIPEC (Tumor)	KRT20	22909
42	HIPEC (Tumor)	KRT20	6419
19	Bariatric (normal)	CCAT1	2.6
20	Bariatric (normal)	CCAT1	1.0[a]
30	Bariatric (normal)	KRT20	1.0[a]
31	Bariatric (normal)	KRT20	1.0[a]

[a] CCAT1 and KRT20 levels were normalized to CCAT1 and KRT20 RNA levels found in bariatric (normal) tissues.

tissues, half of the bariatric tissues were frozen and analyzed by qRT-PCR for both RNA transcripts (Table 2 and Supplementary Table 3S for repeated experiments). Extremely low (undetermined) expression levels of CCAT1 and KRT20 were found as expected. As an additional negative control, the non-targeted FIT-PNA (Supplementary Table S1) was examined. This FIT-PNA was sprayed (2.5 μM) on fresh HIPEC tumor tissues (Fig. 3e and f). No fluorescent signal was observed further highlighting the sequence specificity of FIT-PNAs to their RNA targets.

To date, the BisQ cyanine dye is the most red-shifted mono-methine cyanine dye used as a surrogate base in FIT-PNA probes (Kolevzon et al., 2016). Given its red-shifted fluorescence (λ_{max},exc = 605–610 nm) we tested FIT-PNAs in-depth fluorescence in fresh tumor tissues (Fig. 4a and Fig. 4b for both CCAT1 and KRT20 RNA transcripts, respectively). Movies for both FIT-PNAs are shown in supporting information (Supplementary Video S1 and Video S2). Spraying KRT20-FIT-PNA (Fig. 4a) and then following fluorescence by a two-photon microscope revealed a 240-μm penetration/detection as corroborated by fluorescence imaging (images taken at 5 μm sections). Similarly, CCAT1-FIT-PNA (Fig. 4b) was detected up to 165 μm in depth after spraying FIT-PNA on fresh tumor tissue. These results reveal the further potential of such FIT-PNAs not only for imaging the surface of the tumor. Obviously, a near infrared mono-methine cyanine dye would be an ideal choice as a FIT-PNA surrogate base for in-depth imaging; a task we are currently striving to achieve.

Supplementary video related to this article can be found at https://

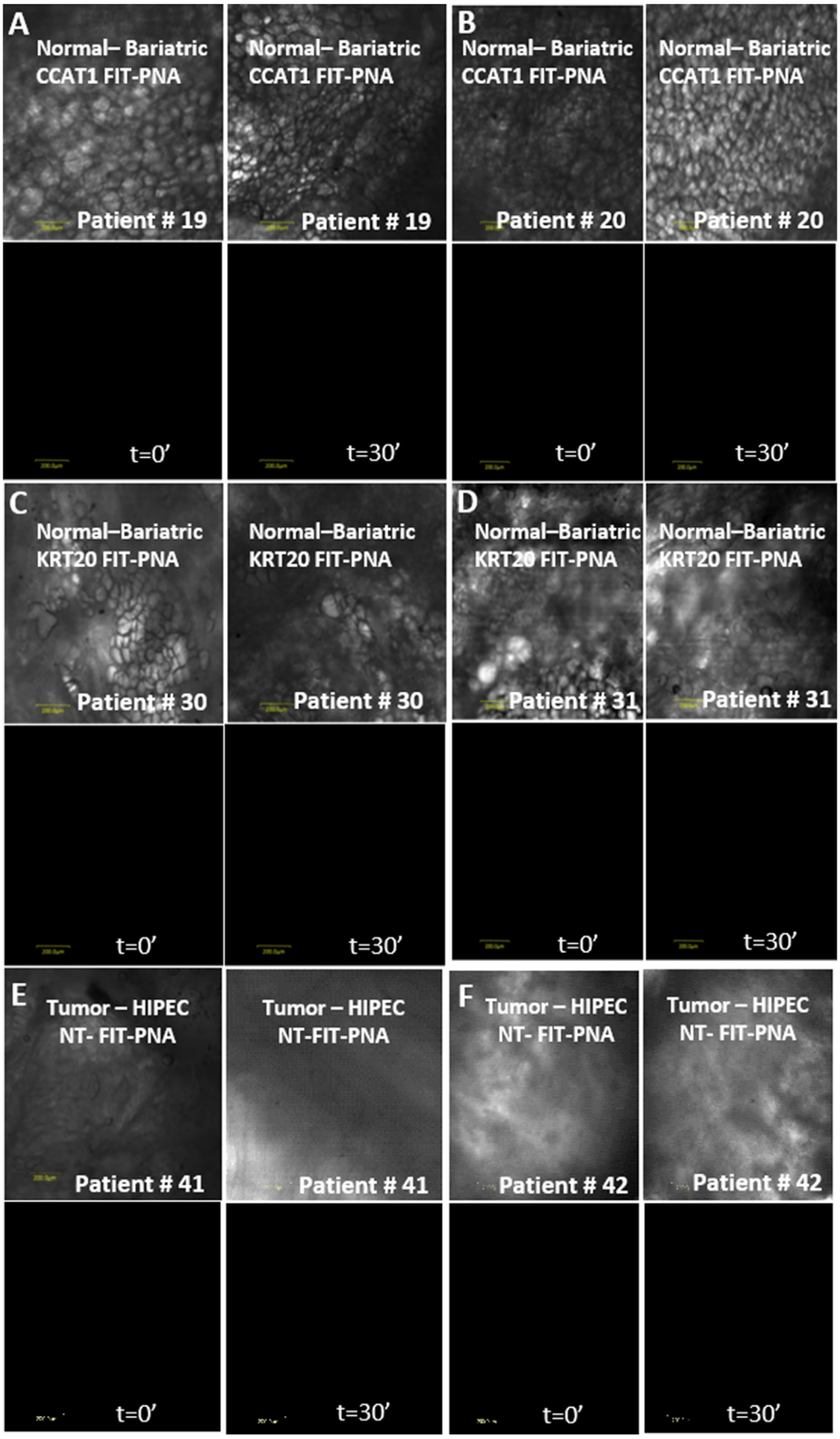

Fig. 3. FIT-PNAs are tumor (sequence) specific. a) and b) Bariatric normal fresh tissue from 2 patients after spraying tissues with 2.5 μM CCAT-FIT-PNA. c) and d) Bariatric normal fresh tissue from 2 patients after spraying tissues with 2.5 μM KRT20-FIT-PNA. e) and f) Peritoneal metastatic tissue after CRS/HIPEC from 2 patients after spraying tissues with 2.5 μM non-targeted FIT-PNA. Scale bar – 200 μm.

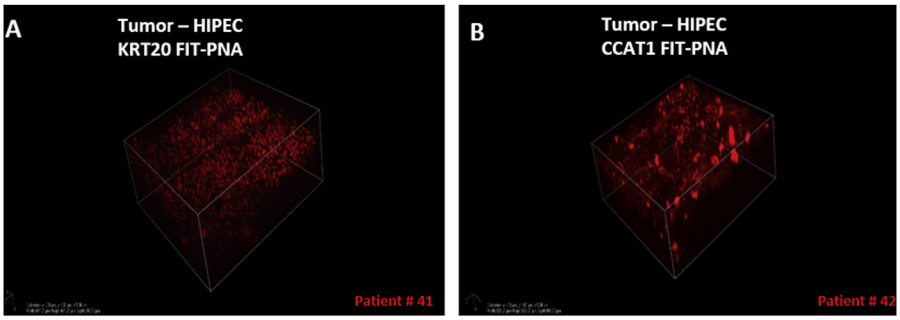

Fig. 4. FIT-PNAs penetrate fresh human tumor tissue. Peritoneal metastatic tissue after CRS-HIPEC from 2 patients after spraying tissues with (a) 2.5 μM KRT20-FIT-PNA, and b) 2.5 μM CCAT1-FIT-PNA. 3D images were acquired by imaging layer by layer at 5-μm intervals. A depth of up to 240 and 185 μm where the fluorescent signal was visualized, is achieved for KRT20-FIT-PNA and CCAT1-FIT-PNA, respectively.

doi.org/10.1016/j.bios.2019.04.056.

4. Discussion

The presence of residual tumor tissue (defined as 'occult residual disease') after surgery has been reported in a variety of surgical procedures with high-grade glioma resections reaching 65% of cases (Stummer et al., 2006). This highlights the need for an accompanying diagnostic procedure to detect these occult tumor deposits. Most FGS procedures rely on systemic administration of the fluorophore; whether targeted or non-targeted. This, in turn, may result in systemic toxicity and requires pre-injection of the sensing molecule prior to surgery. This pre-injection time frame is not always ideal and may differ from patient to patient. In contrast, the direct application of the sensing molecule on the interrogated tissue may provide a simple and more precise mode to delineate residual tumor tissue. In this regard, we are aware of very few examples where a direct application on the tissue has been realized. Urano and co-workers (Urano et al., 2011) devised a gamma glutamyl transpeptidase (GGT)-activated fluorophore that generated a distinct green fluorescent signal in an ovarian cancer mouse model within minutes, post spraying this targeted probe. Other GGT-activated fluorophores have been implicated in intraoperative imaging of various cancers such as breast cancer (Ueo et al., 2015), colon cancer (Ou-Yang et al., 2019), and liver cancer (Miyata et al., 2017; Ou-Yang et al., 2019). Notably, some recent GGT-activated probes have been shown to perform in the Near-IR region (Iwatate et al., 2018); providing deep tissue imaging.

The Bogyo lab (Segal et al., 2015) devised a quenched fluorescent activity-based probe (qABP) for cysteine Cathepsins that fluorescently labelled fresh frozen human polyps from colon cancer patients. Both probe types (qABP and GGT) are activated by enzymatic reactions and may be limited by nonspecific activation in inflammation. To the best of our knowledge, this report presents the first example where RNA biomarkers associated with cancer are directly detected by FIT-PNAs on fresh (non-fixed) human cancer tissues. The fast and clear fluorescent signal generated after simple spraying of CCAT1 FIT-PNA highlights the potential of such probes. In addition, PNA molecules have been studied in-vivo and have been documented as well tolerated with minimal toxicity (Rembach et al., 2004). In our approach, spraying FIT-PNA directly on the suspected tissue as opposed to systemic administration of the probe would have a significant advantage in terms of potential systemic toxicity. Although the KRT20 FIT-PNA was not as bright and required a 30 min incubation period for an appreciable fluorescent response in tumor tissues, it indicates that one may design other FIT-PNAs to other RNA cancer biomarkers. It is reasonable to suggest that as long as one designs a FIT-PNA with structural features as those presented in Scheme 1 (i.e. a short peptide of four (D)-Lysines, BisQ as the cyanine dye situated in the central region of the PNA sequence, and a PNA sequence that is a well–established target for the specific RNA biomarker of choice), it is possible to detect a variety of over-expressed oncogenic RNA biomarkers for a variety of cancers (Xie et al., 2018). For example, in CRC, one could design a FIT-PNA to detect the lncRNA MALTA1 (Li et al., 2017) or miR-191 (Guo et al., 2018), and for breast cancer, the lncRNA LINP1 (Liang et al., 2018).

Moreover, this approach is not limited to cancer diagnosis. For example, inflammation in tissue may be detected (and discriminated from tumor tissue) by designing a FIT-PNA for detecting miR-146 (Taganov et al., 2006). This highlights the general use of such FIT-PNAs to detect RNA biomarkers in fresh tissues.

5. Conclusions

In summary, we have developed FIT-PNAs with a red-emitting base surrogate (BisQ) targeting the oncogenic CCAT1 lncRNA and KRT20 mRNA. Both KRT20 CCAT1 FIT-PNAs are brightly fluorescent after direct topical application (spraying) of these molecules on fresh cancerous tissue, with CCAT1 FIT-PNA generating a fluorescent signal in a matter of minutes. Such molecular probes may be promising candidates for clinical translation.

Conflicts of interest statement

The authors declare that they have no conflicts of interest.

CRediT authorship contribution statement

Dina Hashoul: Investigation, Methodology. **Rachel Shapira:** Formal analysis. **Maria Falchenko:** Investigation, Methodology. **Odelia Tepper:** Methodology. **Vera Paviov:** Methodology. **Aviram Nissan:** Conceptualization. **Eylon Yavin:** Conceptualization, Writing - original draft, Writing - review & editing.

Acknowledgments

This work was supported by the Israel Science Foundation (grant No. 476/17) and the Israel Innovation Authority (grant No. 55330). We thank Prof. Abraham Rubinstein for his useful insights. EY acknowledges the David R. Bloom Center for Pharmacy and the Alex Grass Center for Drug Design and Novel Therapeutics for financial support.

Appendix A. Supplementary data

Supplementary data to this article can be found online at https://doi.org/10.1016/j.bios.2019.04.056.

References

Alaiyan, B., Ilyayev, N., Stojadinovic, A., Izadjoo, M., Roistacher, M., Pavlov, V., Tzivin, V., Halle, D., Pan, H.G., Trink, B., Gure, A.O., Nissan, A., 2013. Differential expression of colon cancer associated transcript1 (CCAT1) along the colonic adenoma-carcinoma sequence. BMC Canc. 13.

Bethge, L., Jarikote, D.V., Seitz, O., 2008. New cyanine dyes as base surrogates in PNA: forced intercalation probes (FIT-probes) for homogeneous SNP detection. Bioorg. Med. Chem. 16 (1), 114–125.

Deng, L., Yang, S.B., Xu, F.F., Zhang, J.H., 2015. Long noncoding RNA CCAT1 promotes hepatocellular carcinoma progression by functioning as a let-7 sponge. J. Exp. Clin. Cancer Res. 34.

Dsouza, A.V., Lin, H.Y., Henderson, E.R., Samkoe, K.S., Pogue, B.W., 2016. Review of fluorescence-guided surgery systems: identification of key performance capabilities beyond indocyanine green imaging. J. Biomed. Opt. 21 (8).
Futamura, M., Takagi, Y., Koumura, H., Kida, H., Tanemura, H., Shimokawa, K., Saji, S., 1998. Spread of colorectal cancer micrometastases in regional lymph nodes by reverse transcriptase-polymerase chain reactions for carcinoembryonic antigen and cytokeratin 20. J. Surg. Oncol. 68 (1), 34–40.
Guo, X.Q., Hua, Y.M., 2017. CCAT1: an oncogenic long noncoding RNA in human cancers. J. Cancer Res. Clin. Oncol. 143 (4), 555–562.
Guo, Z., Liu, Z., Yue, H., Wang, J., 2018. Beta-elemene increases chemosensitivity to 5-fluorouracil through down-regulating microRNA-191 expression in colorectal carcinoma cells. J. Cell. Biochem. 119 (8), 7032–7039.
Hague, A., Faizi, M.S.H., Rather, J.A., Khan, M.S., 2017. Next generation NIR fluorophores for tumor imaging and fluorescence-guided surgery: a review. Bioorg. Med. Chem. 25 (7), 2017–2034.
Harlaar, N.J., Koller, M., de Jongh, S.J., van Leeuwen, B.L., Hemmer, P.H., Kruijff, S., van Ginkel, R.J., Been, L.B., de Jong, J.S., Kats-Ugurlu, G., Linssen, M.D., Jorritsma-Smit, A., van Oosten, M., Nagengast, W.B., Ntziachristos, V., van Dam, G.M., 2016. Molecular fluorescence-guided surgery of peritoneal carcinomatosis of colorectal origin: a single-centre feasibility study. Lancet Gastroenterol. Hepatol. 1 (4), 283–290.
Hoevelmann, F., Gaspar, I., Chamiolo, J., Kasper, M., Steffen, J., Ephrussi, A., Seitz, O., 2016. LNA-enhanced DNA FIT-probes for multicolour RNA imaging. Chem. Sci. 7 (1), 128–135.
Hoevelmann, F., Gaspar, I., Loibl, S., Ermilov, E.A., Roeder, B., Wengel, J., Ephrussi, A., Seitz, O., 2014. Brightness through local constraint-LNA-enhanced FIT hybridization probes for in vivo ribonucleotide particle tracking. Angew. Chem. Int. Ed. 53 (42), 11370–11375.
Huarte, M., 2015. The emerging role of lncRNAs in cancer. Nat. Med. 21 (11), 1253–1261.
Iwatate, R.J., Kamiya, M., Umezawa, K., Kashima, H., Nakadate, M., Kojima, R., Urano, Y., 2018. Silicon rhodamine-based near-infrared fluorescent probe for γ-glutamyltransferase. Bioconjug. Chem. 29 (2), 241–244.
Ji, P., Diederichs, S., Wang, W.B., Boing, S., Metzger, R., Schneider, P.M., Tidow, N., Brandt, B., Buerger, H., Bulk, E., Thomas, M., Berdel, W.E., Serve, H., Muller-Tidow, C., 2003. MALAT-1, a novel noncoding RNA, and thymosin beta 4 predict metastasis and survival in early-stage non-small cell lung cancer. Oncogene 22 (39), 8031–8041.
Kam, Y., Rubinstein, A., Naik, S., Djavsarov, I., Halle, D., Ariel, I., Gure, A.O., Stojadinovic, A., Pan, H.G., Tsivin, V., Nissan, A., Yavin, E., 2014. Detection of a long non-coding RNA (CCAT1) in living cells and human adenocarcinoma of colon tissues using FIT-PNA molecular beacons. Cancer Lett. 352 (1), 90–96.
Koehler, O., Jarikote, D.V., Seitz, O., 2005. Forced intercalation probes (FIT probes): Thiazole orange as a fluorescent base in peptide nucleic acids for homogeneous single-nucleotide-polymorphism detection. Chembiochem 6 (1), 69–77.
Kolevzon, N., Hashoul, D., Naik, S., Rubinstein, A., Yavin, E., 2016. Single point mutation detection in living cancer cells by far-red emitting PNA-FIT probes. Chem. Commun. 52 (11), 2405–2407.
Kovaliov, M., Segal, M., Fischer, B., 2013. Fluorescent p-substituted-phenyl-imidazolo-cytidine analogues. Tetrahedron 69 (18), 3698–3705.
Kummer, S., Knoll, A., Socher, E., Bethge, L., Herrmann, A., Seitz, O., 2011. Fluorescence imaging of Influenza H1N1 mRNA in living infected cells using single-chromophore FIT-PNA. Angew. Chem. Int. Ed. 50 (8), 1931–1934.
Kummer, S., Knoll, A., Socher, E., Bethge, L., Herrmann, A., Seitz, O., 2012. PNA FIT-probes for the dual color imaging of two viral mRNA targets in Influenza H1N1 infected live cells. Bioconjug. Chem. 23 (10), 2051–2060.
Li, P., Zhang, X., Wang, H., Wang, L., Liu, T., Du, L., Yang, Y., Wang, C., 2017. MALAT1 is associated with poor response to oxaliplatin-based chemotherapy in colorectal cancer patients and promotes chemoresistance through EZH2. Mol. Canc. Therapeut. 16 (4), 739–751.
Liang, Y., Li, Y., Song, X., Zhang, N., Sang, Y., Zhang, H., Liu, Y., Chen, B., Zhao, W., Wang, L., Guo, R., Yu, Z., Yang, Q., 2018. Long noncoding RNA LINP1 acts as an oncogene and promotes chemoresistance in breast cancer. Cancer Biol. Ther. 19 (2), 120–131.
Liu, S.-P., Yang, J.-X., Cao, D.-Y., Shen, K., 2013. Identification of differentially expressed long non-coding RNAs in human ovarian cancer cells with different metastatic potentials. Cancer Biol. Med. 10 (3), 138–141.
Low, P.S., Singhal, S., Srinivasarao, M., 2018. Fluorescence-guided surgery of cancer: applications, tools, and perspectives. Curr. Opin. Chem. Biol. 45, 64–72.
Luo, J., Tang, L., Zhang, J., Ni, J., Zhang, H.-p., Zhang, L., Xu, J.-f., Zheng, D., 2014. Long non-coding RNA CARLo-5 is a negative prognostic factor and exhibits tumor pro-oncogenic activity in non-small cell lung cancer. Tumor Biol. 35 (11), 11541–11549.
Ma, C., Shi, X., Zhu, Q., Li, Q., Liu, Y., Yao, Y., Song, Y., 2016. The growth arrest-specific transcript 5 (GAS5): a pivotal tumor suppressor long noncoding RNA in human cancers. Tumor Biol. 37 (2), 1437–1444.
Ma, M.Z., Chu, B.F., Zhang, Y., Weng, M.Z., Qin, Y.Y., Gong, W., Quan, Z.W., 2015. Long non-coding RNA CCAT1 promotes gallbladder cancer development via negative modulation of miRNA-218-5p. Cell Death Dis. 6.
Miyata, Y., Ishizawa, T., Kamiya, M., Yamashita, S., Hasegawa, K., Ushiku, A., Shibahara, J., Fukayama, M., Urano, Y., Kokudo, N., 2017. Intraoperative imaging of hepatic cancers using γ-glutamyltranspeptidase-specific fluorophore enabling real-time identification and estimation of recurrence. Sci. Rep. 7 (1) 3542-3542.
Nissan, A., Stojadinovic, A., Mitrani-Rosenbaum, S., Halle, D., Grinbaum, R., Roistacher, M., Bochem, A., Dayanc, B.E., Ritter, G., Gomceli, I., Bostanci, E.B., Akoglu, M., Chen, Y.-T., Old, L.J., Gure, A.O., 2012. Colon cancer associated transcript-1: a novel RNA expressed in malignant and pre-malignant human tissues. Int. J. Cancer 130 (7), 1598–1606.
Ou-Yang, J., Li, Y., Jiang, W.-L., He, S.-Y., Liu, H.-W., Li, C.-Y., 2019. Fluorescence-guided cancer diagnosis and surgery by a zero cross-talk ratiometric near-infrared γ-glutamyltranspeptidase fluorescent probe. Anal. Chem. 91 (1), 1056–1063.
Rembach, A., Turner, B.J., Bruce, S., Cheah, I.K., Scott, R.L., Lopes, E.C., Zagami, C.J., Beart, P.M., Cheung, N.S., Langford, S.J., Cheema, S.S., 2004. Antisense peptide nucleic acid targeting GluR3 delays disease onset and progression in the SOD1 G93A mouse model of familial ALS. J. Neurosci. Res. 77 (4), 573–582.
Segal, E., Prestwood, T.R., van der Linden, W.A., Carmi, Y., Bhattacharya, N., Withana, N., Verdoes, M., Habtezion, A., Engleman, E.G., Bogyo, M., 2015. Detection of intestinal cancer by local, topical application of a quenched fluorescence probe for cysteine Cathepsins. Chem. Biol. 22 (1), 148–158.
Silva, G.L., Ediz, V., Yaron, D., Armitage, B.A., 2007. Experimental and computational investigation of unsymmetrical cyanine dyes: understanding torsionally responsive fluorogenic dyes. J. Am. Chem. Soc. 129 (17), 5710–5718.
Soeth, E., Roder, C., Juhl, H., Kruger, U., Kremer, B., Kalthoff, H., 1996. The detection of disseminated tumor cells in bone marrow from colorectal-cancer patients by a cytokeratin-20-specific nested reverse-transcriptase-polymerase-chain reaction is related to the stage of disease. Int. J. Cancer 69 (4), 278–282.
Sonar, M.V., Wampole, M.E., Jin, Y.-Y., Chen, C.-P., Thakur, M.L., Wickstrom, E., 2014. Fluorescence detection of KRAS2 mRNA hybridization in lung cancer cells with PNA-peptides containing an internal Thiazole orange. Bioconjug. Chem. 25 (9), 1697–1708.
Stummer, W., Pichlmeier, U., Meinel, T., Wiestler, O.D., Zanella, F., Hans-Jurgen, R., Ala-Glioma Study, G., 2006. Fluorescence-guided surgery with 5-aminolevulinic acid for resection of malignant glioma: a randomied controlled multicentre phase III trial. Lancet Oncol. 7 (5), 392–401.
Taganov, K.D., Boldin, M.P., Chang, K.J., Baltimore, D., 2006. NF-kappaB-dependent induction of microRNA miR-146, an inhibitor targeted to signaling proteins of innate immune responses. Proc. Natl. Acad. Sci. U.S.A. 103 (33), 12481–12486.
Torres, A.G., Fabani, M.M., Vigorito, E., Williams, D., Al-Obaidi, N., Wojciechowski, F., Hudson, R.H.E., Seitz, O., Gait, M.J., 2012. Chemical structure requirements and cellular targeting of microRNA-122 by peptide nucleic acids anti-miRs. Nucleic Acids Res. 40 (5), 2152–2167.
Ueo, H., Shinden, Y., Tobo, T., Gamachi, A., Udo, M., Komatsu, H., Nambara, S., Saito, T., Ueda, M., Hirata, H., Sakimura, S., Takano, Y., Uchi, R., Kurashige, J., Akiyoshi, S., Iguchi, T., Eguchi, H., Sugimachi, K., Kubota, Y., Kai, Y., Shibuta, K., Kijima, Y., Yoshinaka, H., Natsugoe, S., Mori, M., Maehara, Y., Sakabe, M., Kamiya, M., Kakareka, J.W., Pohida, T.J., Choyke, P.L., Kobayashi, H., Ueo, H., Urano, Y., Mimori, K., 2015. Rapid intraoperative visualization of breast lesions with gamma-glutamyl hydroxymethyl rhodamine green. Sci. Rep. 5, 12080.
Urano, Y., Sakabe, M., Kosaka, N., Ogawa, M., Mitsunaga, M., Asanuma, D., Kamiya, M., Young, M.R., Nagano, T., Choyke, P.L., Kobayashi, H., 2011. Rapid cancer detection by topically spraying a gamma-glutamyltranspeptidase-activated fluorescent probe. Sci. Transl. Med. 3 (110).
Verwaal, V.J., van Ruth, S., de Bree, E., van Slooten, G.W., van Tinteren, H., Boot, H., Zoetmulder, F.A.N., 2003. Randomized trial of cytoreduction and hyperthermic intraperitoneal chemotherapy versus systemic chemotherapy and palliative surgery in patients with peritoneal carcinomatosis of colorectal cancer. J. Clin. Oncol. 21 (20), 3737–3743.
Wang, C.S., Wang, Z.H., Zhao, T., Li, Y., Huang, G., Sumer, B.D., Gao, J.M., 2018. Optical molecular imaging for tumor detection and image-guided surgery. Biomaterials 157, 62–75.
Wyld, D.K., Selby, P., Perren, T.J., Jonas, S.K., Allen-Mersh, T.G., Wheeldon, J., Burchill, S.A., 1998. Detection of colorectal cancer cells in peripheral blood by reverse-transcriptase polymerase chain reaction for cytokeratin 20. Int. J. Cancer 79 (3), 288–293.
Xie, M., Ma, L., Xu, T., Pan, Y., Wang, Q., Wei, Y., Shu, Y., 2018. Potential regulatory roles of microRNAs and long noncoding RNAs in anticancer therapies. Mol. Ther. Nucleic Acids 13, 233–243.
Xin, Y., Li, Z., Shen, J.X., Chan, M.T.V., Wu, W.K.K., 2016. CCAT1: a pivotal oncogenic long non-coding RNA in human cancers. Cell Prolif 49 (3), 255–260.
Zhang, R.R., Schroeder, A.B., Grudzinski, J.J., Rosenthal, E.L., Warram, J.M., Pinchuk, A.N., Eliceiri, K.W., Kuo, J.S., Weichert, J.P., 2017. Beyond the margins: real-time detection of cancer using targeted fluorophores. Nat. Rev. Clin. Oncol. 14 (6), 347–364.
Zhang, X.F., Liu, T., Li, Y., Li, S., 2015. Overexpression of long non-coding RNA CCAT1 is a novel biomarker of poor prognosis in patients with breast cancer. Int. J. Clin. Exp. Pathol. 8 (8), 9440–9445.
Zhang, Y., Ma, M., Liu, W., Ding, W., Yu, H., 2014. Enhanced expression of long non-coding RNA CARLo-5 is associated with the development of gastric cancer. Int. J. Clin. Exp. Pathol. 7 (12), 8471–8479.